

---

# Interpretable and Personalized Apprenticeship Scheduling: Learning Interpretable Scheduling Policies from Heterogeneous User Demonstrations

---

Rohan Paleja, Andrew Silva, Letian Chen, and Matthew Gombolay

Georgia Institute of Technology

Atlanta, GA 30332

{rohan.paleja, andrew.silva, letian.chen, mgombolay3}@gatech.edu

## Abstract

Resource scheduling and coordination is an NP-hard optimization requiring an efficient allocation of agents to a set of tasks with upper- and lower bound temporal and resource constraints. Due to the large-scale and dynamic nature of resource coordination in hospitals and factories, human domain experts manually plan and adjust schedules on the fly. To perform this job, domain experts leverage heterogeneous strategies and rules-of-thumb honed over years of apprenticeship. What is critically needed is the ability to extract this domain knowledge in a heterogeneous and interpretable apprenticeship learning framework to scale beyond the power of a single human expert, a necessity in safety-critical domains. We propose a personalized and interpretable apprenticeship scheduling algorithm that infers an interpretable representation of all human task demonstrators by extracting decision-making criteria via an inferred, personalized embedding non-parametric in the number of demonstrator types. We achieve near-perfect LfD accuracy in synthetic domains and 88.22% accuracy on a planning domain with real-world, outperforming baselines. Finally, our user study showed our methodology produces more interpretable and easier-to-use models than neural networks ( $p < 0.05$ ).

## 1 Introduction

Coordinating resources in time and space is a challenging and costly problem worldwide, affecting everything from the medical supplies we need to fight pandemics to the food on our tables. The manufacturing and healthcare industries account for a total of \$35 trillion [17] and \$8.1 trillion [27] USD, respectively. In manufacturing, scheduling workers – whether they be humans or robots – to complete a set of tasks in a shared space with upper- and lower-bound temporal constraints (i.e., deadline and wait constraints) is an NP-hard optimization problem [5], typically approaching computational intractability for real-world problems of interest.

Human domain experts efficiently, if sub-optimally, solve these NP-hard problems to coordinate resources using heterogeneous rules-of-thumb and strategies honed over decades of apprenticeship, creating unique heuristics depending on experts' varied experiences and personal preferences [22, 40]. Each expert has her own strategies, and it is common for factories and hospital wards to be run completely differently – yet effectively – across different shifts based upon the person in charge of coordinating the workers' activities [26, 32, 37]. The challenge we pose is to develop new *apprenticeship learning* techniques for capturing these heterogeneous rules-of-thumb in order to scale beyond the power of a single expert. However, such heterogeneity is not readily handled by traditional apprenticeship learning approaches that assume demonstrator homogeneity. A canonical example of this limitation is of human drivers teaching an autonomous car to pass a slower-moving car, where some drivers prefer to pass on the left and others on the right. Apprenticeship learning

approaches assuming homogeneous demonstrations either fit the mean (i.e., driving straight into the car ahead of you) or fit a single mode (i.e., only pass to the left).

The field of apprenticeship learning has recently begun working to relax the assumption of homogeneous demonstrations by explicitly capturing modes in heterogeneous human demonstrations [6, 20, 25, 42]. One such approach, InfoGAIL [25], uses a generative adversarial setting with variational inference to learn discrete, latent codes to describe multi-modal decision-making. However, InfoGAIL requires access to an environment simulator, relies on a ground-truth reward signal, and is ill-suited to reasoning about resource scheduling and optimization problems, as we show in Section 5. Further, modern imitation learning frameworks lack interpretability, hampering adoption in safety-critical and legally-regulated domains [2, 9, 24, 43].

**Contributions** – Overcoming these key limitations of prior work, we develop a novel, data-efficient apprenticeship learning framework for learning from heterogeneous scheduling demonstration. The key to our approach is a neural network architecture that serves as a function approximator specifically designed for sparsity to afford easy “discretization” into a Boolean decision tree after training as well as the ability to leverage variational inference to tease out each demonstrator’s unique decision-making criteria. In Section 5, we empirically validate that our approach, “Personalized Neural Trees”, outperforms baselines even after discretization into a decision tree. Our contributions are as follows:

1. Formulate a personalized and interpretable apprenticeship scheduling framework for heterogeneous LfD that outperforms prior state-of-the-art approaches on both synthetic and real-world data across several domains (+51% and +11%, respectively) through the use of personalized embeddings without constraining the number of demonstrator types.
2. Develop a methodology for converting a personalized neural tree into an interpretable representation that directly translates decision-making behavior. Our discretized trees also outperform previous benchmarks on synthetic and real-world data across several domains.
3. Conduct a user study that shows our post-processed interpretable trees are more interpretable ( $p < 0.05$ ), easier to simulate ( $p < 0.01$ ), and quicker to validate ( $p < 0.01$ ) than their black box neural network counterparts.

## 2 Background

**Preliminaries** – LfD mechanisms are often based on a Markov Decision Process (MDP), a five-tuple  $M = \langle S, A, T, \gamma, R \rangle$  where  $S$  is a set of states,  $A$  is a set of actions,  $T : S \times A \times S \rightarrow [0, 1]$  is a transition function, in which  $T(s, a, s')$  is the probability of being in state  $s'$  after executing action  $a$  in state  $s$ ,  $R : S \rightarrow \mathbb{R}$  (or  $R : S \times A \rightarrow \mathbb{R}$ ) is the reward function, and  $\gamma \in [0, 1]$  is the discount factor. The goal in LfD is to receive both a set of trajectories provided by a human demonstrator  $\{\langle s_t, a_t \rangle, \forall t \in \{1, 2, \dots, T\}\}$  as well as an MDP\( $R$ , and then to recover a policy that can predict the correct state-action sequence a human would take in a novel situation.

**Imitation Learning** – There has been growing interest in tackling decision-maker heterogeneity [12, 16, 20, 25, 28, 31, 42]. Nikolaidis et al. [28] first used an expectation-maximization formulation to cluster decision-maker behavior before applying inverse reinforcement learning (IRL) for each cluster  $k$ . Negatively, this approach requires interaction with an environment model, and the IRL algorithm only has access to  $\sim 1/k^{th}$  of the data to learn from. More recently, Li et al. [25] presented InfoGAIL, which used mutual information maximization to learn discrete, latent codes; however, InfoGAIL requires access to an environment simulator and a ground-truth reward signal. While InfoGAIL argues its latent codes afford interpretability, but its model structure is still a black-box neural network [35]. Hsiao et al. [20] presented an approach to discover latent factors within demonstrations using a categorical latent variable with limited expressivity. Finally, Tamar et al. [42] used a sampling-based approach to learn the modalities within the data, but the approach requires voluminous data due to the algorithm’s high-variance estimation framework.

Researchers have also sought to learn scheduling policies from demonstration [1, 13, 14, 15]. Gombolay et al. [13] considers learning scheduling policies but does not consider heterogeneity. Berry et al. [1] proposed PTIME to learn to schedule calendar appointments; however, this approach requires manually soliciting user ranking data and computationally-intensive nonlinear optimization.

**Differentiable Decision Trees** – To both enable model interpretability and because prior work has shown the power of decision trees for apprenticeship scheduling [13], we seek to harness a decision tree architecture that is amenable to learning latent embeddings capturing heterogeneity. As such, we

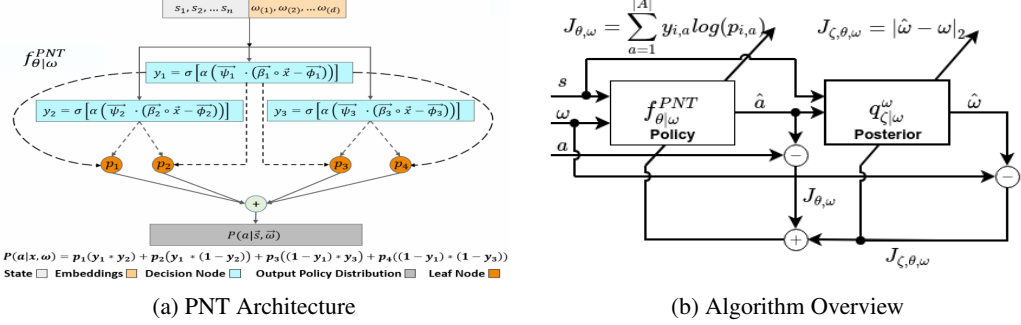


Figure 1: The PNT architecture (left) displaying decision nodes,  $y_i$ , with evaluation equations, leaf nodes,  $k$ , with respective weights  $p_k$ , and output equation describing the calculation of the action PMF. An overview of our training algorithm (right) displaying the input/output flow of the policy and the posterior alongside their respective update equations.

build upon prior work in differentiable decision trees (DDTs) [39, 41] – a neural network architecture that takes the topology of a decision tree. Each decision node,  $i$ , is represented by a sigmoid activation function,  $(1 + e^{-\alpha(\beta_i \vec{s} - \phi_i)})^{-1}$ , where the features vectors describing the current state,  $\vec{s}$ , are weighted by  $\beta_i$ , and a splitting criterion,  $\phi_i$ , is subtracted to form the splitting rule.  $\alpha$  governs the steepness of the activation, where  $\alpha \rightarrow \infty$  results in a step function. As we are learning a policy via apprenticeship learning, we adopt the formulation of [38] for the leaf nodes; i.e., each leaf node,  $k$ , is represented by a probability distribution over discrete actions, denoted  $p_k$ . We describe in Section 3.1 how we extend this formulation of a DDT for our framework.

### 3 Personalized and Interpretable Neural Trees

In this section, we present our apprenticeship framework that utilizes person-specific (personalized) embeddings, learned through backpropagation, which enables the apprenticeship learner to automatically adapt to a person’s unique characteristics while simultaneously leveraging any homogeneity that exists within the data (e.g., uniform adherence to hard constraints).

#### 3.1 Algorithm Overview

To effectively learn from heterogeneous decision-makers, we must capture the homo- and heterogeneity in their demonstrations, allowing us to learn a general behavior model accompanied by personalized embeddings that fit distinct behavior modalities. We contribute a novel apprenticeship learning model for resource scheduling, “Personalized Neural Trees”, by extending DDTs in four important ways: 1) Personalized embeddings,  $\omega$ , as a latent variable representing person-specific modality (Section 3.2), 2) Variational inference mechanism to maximize the mutual information between the embedding and the modeled decision-maker (Section 3.2.1), 3) Counterfactual reasoning to increase data-efficiency (Section 3.2.2), and 4) Novel feature selector,  $\vec{\psi}_i$ , for each decision node to enhance interpretability (Section 3.3).

A Personalized Neural Tree (PNT) learns a model,  $f_{\theta|\omega}^{PNT} : S \times \Omega \rightarrow [0, 1]^{|A|}$ , of human demonstrator decision-making policies, where  $\theta \in \Theta$  are the policy weights and  $\omega \in \Omega$  ( $\Omega \subset \mathbb{R}^d$ ) is the demonstrator-specific personalized embedding of length  $d$ , which is a tunable hyperparameter. Here,  $\Omega = \{\omega_1, \omega_2, \dots, \omega_P\}$  represents the set of all demonstrator personalized embeddings. The person-specific features  $\omega$  identify the latent pattern of thinking for the current decision-maker. We note that the policy weights,  $\theta \in \Theta$ , are specifically defined as  $\Theta = \alpha \times \Psi \times B \times \Phi \times \mathcal{P}$ , where  $\alpha$ ,  $B$ , and  $\Phi$  are the parameters of the decision nodes (Section 3.2),  $\mathcal{P}$  are the leaf parameters (Section 3.2), and  $\Psi$  are a new set of parameters we introduce in Section 3.3 to enhance interpretability during post-training discretization.

Alongside learning a demonstrator’s decision-making policy  $f_{\theta|\omega}^{PNT}$ , we introduce (Section 3.2.1) an information theoretic regularization model, similar to Chen et al. [7], to maximize mutual information between latent embeddings,  $\omega$ , and trajectories,  $\tau$ , by learning a model,  $q_{\zeta|\theta}^{\omega} : S \times [0, 1]^{|A|} \rightarrow \mathcal{N}_{\Omega}$

represented by a neural tree (PNT\(\omega\)) with weights \(\zeta\), that approximates the true posterior  $P(\omega|\tau)$ . This induces the latent personalized embeddings to capture modality within demonstrator trajectories.

### 3.2 Personalized Neural Tree

We present architecture of  $f_{\theta|\omega}^{PNT}$  as shown in Fig. 1a. First, a demonstrator-specific embedding (represented by  $\omega \in \Omega$ ) is concatenated with state  $\vec{s} \in S$  and routed directly to each decision node as  $\vec{x} = [\vec{s}, \vec{\omega}]$ . Each decision node in the PNT is conditioned on three differentiable parameters: weights  $\vec{\beta} \in B$ , comparison values  $\vec{\phi} \in \Phi \subset [0, 1]^{n+d}$ , and selective importance vectors  $\vec{\psi} \in \Psi$ . When input data  $\vec{x}$  is passed to a decision node,  $i$ , the data is weighted by  $\vec{\beta}_i$  and compared against  $\vec{\phi}_i$  as shown in Equation 1, where  $\circ$  is the Hadamard product. The PNT algorithm uses its selective importance vector  $\vec{\psi}_i \in [0, 1]^{|\vec{x}|}$  before weighting by  $\alpha$  and passing through a sigmoid to decide which “rule” is the most helpful to apply for this node;  $y_i$  is the probability of decision node  $i$  evaluating to TRUE.

$$y_i = \sigma[\alpha(\vec{\psi}_i \cdot (\vec{\beta}_i \circ \vec{x} - \vec{\phi}_i))] \quad (1)$$

Section 3.3 describes how this extension of the original formulation [41] enhances interpretability.

Leaf nodes,  $k$ , in the PNT maintain a set of weights over each output class denoted  $\vec{p}_k \in \mathcal{P}$ . Each decision node,  $i$ , along a path from the root to a leaf (i.e., a branch) output probabilities,  $y_i$ , for each such decision node. The branch’s probabilities are multiplied to produce a joint probability of reaching the leaf in that branch given state  $\vec{s}$  and the current demonstrator embedding  $\omega_p$ . Each leaf,  $k$  contains a probability mass function (PMF),  $\vec{p}_k$ , where  $\vec{p}_{k,a}$  is the probability of applying action  $a$  for the branch leading to leaf node,  $k$ . This probability distribution,  $\vec{p}_k$ , for leaf,  $k$ , is multiplied by its corresponding branches’ joint probability. Finally, the products of all leaf vectors with their branch’s joint probability is summed to produce the final network output, a PMF for actions given state,  $s$ , and embedding,  $\omega_p$ . An example is shown in Fig. 1a complete with an equation summarizing the output.

#### 3.2.1 Maximizing Mutual Information

The parameters,  $\zeta$ ,  $\theta$ , and  $\omega$ , are updated via a cross-entropy loss and mutual information maximization loss, as discussed in Section 3.4. Maximizing mutual information encourages  $\omega$  to correlate with semantic features within the data distribution (i.e., mode discovery) [7, 25]. Yet, maximizing mutual information between the trajectories and latent code,  $G(\omega; \tau)$ , is intractable as it requires access to the true posterior,  $P(\omega|\tau)$ . Therefore, researchers employ the evidence lower bound (ELBO) of the mutual information  $G(\omega; \tau)$ , as shown in Equation 2. Maximizing  $G(\omega; \tau)$  incentivizes the policy,  $f_{\theta|\omega}^{PNT}$ , to utilize the latent embedding  $\omega$  as much as possible.

$$\begin{aligned} G(\omega; \tau) &= H(\omega) - H(\omega|\tau) \\ &\geq \mathbb{E}_{\omega_p \sim \mathcal{N}(\mu_p, \sigma_p^2), a \sim f_{\theta|\omega}^{PNT}} [\log(q_{\zeta|\theta}^{\omega}(\omega_p | s_p^t, a_p^t))] + H(\omega) = L_G(f_{\theta|\omega}^{PNT} || q_{\zeta|\theta}^{\omega}) \end{aligned} \quad (2)$$

In our approach, we make use of continuous personalized embeddings which allow for greater expressivity in the embedding space,  $\Omega$ . As such, we utilize a mean-squared error (MSE) loss between a sample from the approximate posterior (modeled as a normal distribution with constant variance) and the current embedding. A derivation of the equivalence between using the MSE and log-likelihood loss to maximize the posterior is attached in the supplementary material.

#### 3.2.2 Counterfactual Reasoning

We further enhance our model’s learning capability through counterfactual reasoning [3, 4, 10, 13, 21, 29, 30]. Based upon the insight in prior work in homogeneous apprenticeship scheduling [13] that counterfactual reasoning was critical for learning scheduling strategies from demonstration, we adopt counterfactual reasoning through pairwise comparisons. We present a novel extension to construct counterfactuals in Equations 3-4 that leverages person-specific embeddings as pointwise terms.

$$z_{a,a'}^{t,p} := [\omega_p, \vec{x}^t, x_a^t - x_{a'}^t], y_{a,a'}^t = 1 \text{ for } \forall a' \in A \setminus a \quad (3)$$

$$z_{a',a}^{t,p} := [\omega_p, \vec{x}^t, x_{a'}^t - x_a^t], y_{a',a}^t = 0 \text{ for } \forall a' \in A \setminus a \quad (4)$$

At each timestep, we observe the decision,  $a$ , that person,  $p$ , made at time  $t$ . From each observation, we then extract 1) the feature vector describing that action,  $x_a^t$ , from state  $s^t$ , 2) the corresponding

feature,  $x_{a'}^t$ , for an alternative action  $\forall a' \in A \setminus a$ , 3) a contextual feature vector capturing features common to all actions,  $\bar{x}^t$ , and 4) the person’s embedding,  $\omega_p$ . We note that each demonstrator has their own embedding which is updated through backpropagation.

$$\hat{P}(a|t, p) \sim \sum_{a' \in A} f(a, a', p) \quad (5)$$

---

**Algorithm 1** PNT Training

---

**Input:** data  $\vec{s} \in S$ , labels  $a \in A$ , embeddings  $\omega \in \Omega$   
**Output:**  $f_{\theta|\omega}^{PNT*}$

```

1: Initialize  $f_{\theta|\omega}^{PNT}$ ,  $q_{\zeta|\theta}^\omega$ ,  $\Omega$ 
2: for i epochs do
3:   Sample data of person  $p$  at time  $t$  :  $\vec{s}_p^t, a_p^t$ 
4:    $\bar{x}_p^t \leftarrow [\omega_p^{(i)}, \vec{s}_p^t]$ 
5:    $\hat{a}_p^t \leftarrow f_{\theta|\omega}^{PNT}(\bar{x}_p^t)$ 
6:    $\mu_p, \sigma_p \leftarrow q_{\zeta|\theta}^\omega(\vec{s}_p^t, \hat{a}_p^t)$ 
7:    $\hat{\omega}_p^{(i)} \sim \mathcal{N}(\mu_p, \sigma_p^2)$ 
8:    $J_{\zeta, \theta, \omega} = |\hat{\omega}_p^{(i)} - \omega_p^{(i)}|$ 
9:    $J_{\theta, \omega} = \text{CrossEntropy}(\hat{a}_p^t || a_p^t)$ 
10:   $J \leftarrow J_{\theta, \omega} + J_{\zeta, \theta, \omega}$ 
11:   $[\omega_p, \theta, \zeta]^{(i+1)} \leftarrow [\omega_p, \theta, \zeta]^{(i)} - \eta \nabla_{\omega_p, \theta, \zeta} J$ 
12: end for

```

---

**Algorithm 2** PNT Run-time Adaptation

---

**Input:** data  $\vec{s}_{p^*}^t \in S$ ,  $f_{\theta|\omega}^{PNT*}$ , training embeddings mean  $\bar{\Omega}$   
**Output:** Demonstrator  $p^*$ ’s action:  $\hat{a}_p^t$

```

1:  $\omega_{p^*}^t = \bar{\Omega}$ 
2: for t in range(1, T) do
3:    $\bar{x}_{p^*}^t = [\omega_{p^*}^t, \vec{s}_{p^*}^t]$ 
4:    $\hat{a}_{p^*}^t \leftarrow f_{\theta|\omega}^{PNT*}(\bar{x}_{p^*}^t)$ 
5:    $a_{p^*}^t \leftarrow \text{ObserveAction}()$ 
6:    $J_{\theta, \omega} = \text{CrossEntropy}(\hat{a}_{p^*}^t || a_{p^*}^t)$ 
7:    $\omega_p^{(t+1)} \leftarrow \omega_p^{(t)} - \eta \nabla_{\theta, \omega} J_{\theta, \omega}$ 
8: end for

```

---

Given this dataset, the apprentice is trained to output a pseudo-probability,  $f(a, a', p)$  of action  $a$  being taken over action  $a'$  at time  $t$  by the human decision-maker  $p$  described by embedding  $\omega_p$ , using features  $z_{a,a'}^{t,p}$ . To predict the probability of taking action  $a$  at timestep  $t$ , we marginalize over all other actions, as shown in Equation 5. Finally, the action prediction is the argument max of this probability,  $\hat{a} = \arg \max_{a \in A} \hat{P}(a|t, p)$ . We term models that use counterfactual reasoning as pairwise models.

**Nota Bene:** While counterfactuals have been exploited in prior work, ours is the first to our knowledge that incorporates variational inference for counterfactual learning from heterogeneous demonstration.

### 3.3 Interpretability via Discretization

In our work, the PNT is able to learn over datasets from heterogeneous demonstrators with high performance while still being able to convert back into a simple, interpretable decision tree post-training. Our formulation, as shown in Equation 1, includes two important augmentations to the original DDT formulation to allow for discretization post-training: 1) The per-node feature selector vector,  $\vec{\psi}_i$ , that learns the relative importance of each candidate splitting rule,  $(\beta_{i,j} x_{i,j} - \phi_{i,j})$  for each feature,  $j$ , and node,  $i$ , and 2) a per-feature splitting criterion,  $\vec{\phi}_{i,j}$ , that enables us to simultaneously curate per-node and per-feature splitting criteria.

During discretization of the PNT to its interpretable form, we apply the following operations to each decision node,  $i$ : 1) Set the argument max of  $\vec{\psi}_i$  to 1 and all other elements to zero; 2) Set  $\alpha \leftarrow \infty$ . For each leaf node,  $i'$ , we likewise set the argument max of  $\vec{\phi}_{i'}$  to one and all non-maximal elements zero. The result of these operations is that each decision node has a single, Boolean splitting rule as per a standard decision tree and each leaf node dictates a single action to be taken. This procedure produces a simple yet powerful decision tree, which we show in Section 5 outperforms all baselines even in its interpretable form.

### 3.4 Training and Runtime Procedure

**Offline** – At the start of training (Algorithm 1), each  $\omega_p$  is a vector of uniform values. A state is sampled,  $\vec{s}_p^t$  at time  $t$ , for demonstrator  $p$ , as well as the person-specific embedding,  $\omega_p^{(i)}$  at training iteration  $i$ , to produce a concatenated input,  $\bar{x}_p^t$  as shown in lines 3 and 4. Policy  $f_{\theta|\omega}^{PNT}$  uses input  $\bar{x}_p^t$  to predict the demonstrator’s action in that state,  $\hat{a}_p^t$ , as shown in line 5. The predicted action,  $\hat{a}_p^t$ , and state,  $\vec{s}_p^t$ , are then used to recover a normal distribution,  $\mathcal{N}(\vec{\mu}_p, \vec{\sigma}_p^2)$ , representing that user’s

personalized embedding  $\omega_p^{(i)}$ . By sampling from this distribution,  $\hat{\omega}_p^{(i)} \sim \mathcal{N}(\vec{\mu}_p, \vec{\sigma}_p^2)$ , we can estimate the accuracy of our approximate posterior by computing the difference between the current embedding and the sampled embedding shown in lines 6 and 7. The learning from demonstration loss is then computed as the cross entropy loss between the true action  $a_p^t$  and the predicted action  $\hat{a}_p^t$ . Summed together, we have a total loss  $J$  that is dependent on  $\zeta$ ,  $\theta$ , and  $\omega$ , as shown in lines 7-10. This loss is then used to update model parameters  $\theta$ , personalized embedding  $\omega$ , and embedding regularization parameters  $\zeta$  via SGD [33], as shown in line 11. This process is repeated until a convergence criterion is satisfied. An overview of this training procedure is displayed in Fig. 1b.

**Online** – When applying the algorithm during runtime for a new human demonstrator,  $p'$ , the model updates the embedding,  $\omega_{p'}$ ; however,  $\theta$  remain static. This online update utilizes the information provided after every timestep (i.e., the true action) to converge on the type of current demonstrator in embedding space. The personalized embedding  $\omega_{p'}$  for a new human demonstrator is initialized to the mean of the embeddings of demonstrators in the training set and updated as we gain more information, as shown in Algorithm 2.

**Interpretable Policy** – Once this tuning process has finished, the person-specific policy can be converted into an interpretable tree, through discretization of our PNTs.

**Covariate Shift** – To remedy the co-variate shift typically encountered with policy-based apprenticeship learning, DAgger [34] was proposed for problems where there is access to the environment. In Section 5, we show that pre-training with PNTs leads to a significant increase in performance for DAgger-based training while also reducing the number of environment samples DAgger requires.

## 4 Evaluation Environments

We utilize three environments to evaluate the utility of our personalized apprenticeship scheduling framework. Additional details about each domain are provided in the supplementary material.

**1) Synthetic Low-Dimensional Environment** The synthetic low-dimensional environment represents a simple domain where an expert will choose an action based on the state and one of two hidden heuristics. This domain captures the idea that we have homogeneity in conforming to constraints  $z$  and strategies or preferences (heterogeneity) in the form of  $\lambda$ . Demonstration trajectories are given in sets of 20 (which we denote a complete schedule), where each observation consists of  $x^t \in \{0, 1\}$  and  $z^t \in \mathcal{N}(0, 1)$ , and the binary output is  $y^t$ . Exact specifications for the computation of the label are given by the observation of  $y = x * \mathbb{1}_{(z>=0 \wedge \lambda=1) \vee (z<0 \wedge \lambda=2)}$ , where  $\mathbb{1}$  is the indicator function.

**2) Synthetic Scheduling Environment** The second environment we use is a synthetic environment that we can control, manipulate, and interpret to empirically validate the efficacy of our proposed method. For our investigation, we leverage a jobshop scheduling environment built on the **XD[ST-SR-TA]** scheduling domain defined by Korsah [23], representing one of the hardest scheduling problems. In this environment, two agents must work together to complete a set of 20 tasks that have upper- and lower-bound temporal constraints (i.e., deadline and wait constraints), proximity constraints, and travel-time constraints. Schedulers have a randomly-generated task-prioritization scheme dependent upon task deadline, distance, and index. The decision-maker must decide the optimal sequence of actions according to the decision-maker’s own criteria. This domain is a more complex variant of the domain in Gombolay et al. [13] as we have demonstrations of heterogeneous scheduling strategies.

**3) Real-world Data: Taxi Domain** We evaluate our algorithm with actual human decision-making behavior collected in a variant of the Taxi Domain in [8]. This domain describes a **ND[ST-SR-TA]** scheduling domain as defined by Korsah [23]. Our environment has three locations: the village, the airport, and the city. The taxi driver has the objective of picking up a passenger from the city or village. A dataset of 70 human-collected tree policies to solve this task (given with leaf node actions such as “Drive to X” and “Wait for Passenger”, and decision node criterion depending on the amount of wait time, traffic time, and current location) are used to generate heterogeneous trajectories.

<sup>1</sup>To infer the embeddings for the interpretable form of our PNT model, we utilize a pre-discretized version of the PNT to learn a demonstrator’s embeddings, which is run prior or concurrently with the discretized version.

<sup>2</sup>An offline version of InfoGAIL [25] is used, as access to a simulator and ground truth reward signal,  $R$ , is not available in many real-world domains.

Table 1: A comparison of heterogeneous LfD approaches. Our method achieves superior performance. Interpretable approaches are shown in the right-hand table.

Method	Low-Dim	Scheduling	Taxi	Method	Low-Dim	Scheduling	Taxi
<b>Our Method</b>	<b><math>97.30 \pm 0.3\%</math></b>	<b><math>96.13 \pm 2.3\%</math></b>	<b><math>88.22 \pm 0.6\%</math></b>	<b>Our Method (Interpretable)</b>	<b><math>96.13 \pm 2.5\%</math></b>	<b><math>99.66 \pm 0.5\%</math></b>	$77.73 \pm 1.9\%$
Sammut et al.	$55.36 \pm 1.2\%$	$5.00 \pm 0.0\%$	$76.16 \pm 0.3\%$	<b>Our Method (DT + <math>\omega</math>)</b>	$53.66 \pm 2.4\%$	$32.85 \pm 0.1\%$	<b><math>87.85 \pm 0.5\%</math></b>
Nikolaidis et al.	$54.23 \pm 2.5\%$	$5.00 \pm 0.0\%$	$76.16 \pm 0.3\%$	Gombolay et al.	$55.76 \pm 1.4\%$	$45.50 \pm 2.0\%$	$75.88 \pm 0.7\%$
Tamar et al.	$55.83 \pm 0.6\%$	$9.78 \pm 0.3\%$	$60.93 \pm 2.8\%$	Vanilla DT	$55.76 \pm 1.4\%$	$32.4 \pm 0.7\%$	$74.90 \pm 0.2\%$
Hsiao et al.	$56.06 \pm 1.1\%$	$11.25 \pm 0.1\%$	$76.19 \pm 0.4\%$				
InfoGAIL	$54.66 \pm 3.4\%$	$25.72 \pm 5.5\%$	$75.51 \pm 0.8\%$				
DDT	$55.28 \pm 1.8\%$	$52.35 \pm 0.7\%$	$76.70 \pm 0.7\%$				

## 5 Results and Discussion

We benchmark our approach against a variety of baselines [13, 20, 25, 28, 36, 42]<sup>2</sup>. Accuracy is the  $k$ -fold cross-validation, multi-class, classification accuracy for state-action pairs.

**1) Synthetic Low-Dimensional Environment** – Table 1 shows that our method for learning a continuous, personalized embedding sets the state-of-the-art ( $95.30\% \pm 0.3\%$ ) for solving this latent-variable classification problem. Even after discretizing to an interpretable form, our method is still able to outperform all baselines, achieving a  $96.13\% \pm 2.49\%$  accuracy. A graphical depiction of the interpretable PNT model, generated through discretization is provided in the supplementary.

**2) Synthetic Scheduling Environment** – Table 1 shows that our personalized apprenticeship learning framework outperforms all other approaches, achieving  $96.13\% \pm 2.3\%$  accuracy in predicting demonstrator actions before conversion to an interpretable policy. After discretizing to an interpretable form, our method is able to achieve  $99.66\% \pm 0.5\%$  accuracy<sup>1</sup>. Furthermore, benchmarks that seek to handle heterogeneity [20, 25, 42] are unable to handle the complexity associated with resource coordination problems, with InfoGAIL achieving only  $25.72\% \pm 5.5\%$  accuracy. We provide a sensitivity analysis for this domain within our supplementary material by considering noisy demonstrations and varying the amount of data available to train the algorithm.

**3) Real-world Data: Taxi Domain** – As seen in Table 1, our personalized apprenticeship learning framework outperforms all other benchmarks and is the only method to achieve over 80%. Even after discretizing to an interpretable form, our method again outperforms all baselines from prior work. We posit that all other methods overfit to the most prevalent behavior, and are unable to tease out the heterogeneity represented within the training dataset.

**Interpretability** – We validate the effectiveness of using the discretized PNT architecture versus several interpretable architectures in Table 1. In two out of three of our environments, using our discretized PNT architecture results in a large performance gain (42.57% in the low-dim and 38.01% in the scheduling environment). In one domain, our method for distilling a DT using our PNT architecture’s learned embeddings appended to the states for training a DT policy was better.

**Understanding Performance of Baselines** – Each baseline has particular flaws that results in its low performance on scheduling problems. Sammut et al. [36] simply assumes homogeneity and serves as a lowerbound. Nikolaidis et al. [28] has two-step approach that first clusters to find modes and then trains policies; thus, there is no feedback symbol to adjust clustering-established modes. Tamar et al. [42] utilizes a sampling-based approach which is acknowledged to require larger data sets. Hsiao et al. [20] uses a categorical variable for modes results in limited expressiveness. InfoGAIL [25] does not have access to a ground-truth reward signal nor the environment. Our approach is the only method that both includes a decision tree-like architecture, helpful for apprenticeship scheduling [13], while also allowing for variational inference.

**Performance of Pretrained Policies with DAgger** – In deploying our pretrained policies within the scheduling environment, our metrics to verify whether our pre-trained PNT (PT-PNT) policies with DAgger are able to outperform randomly-initialized PNT (RI-PNT) policies with DAgger are 1) to maximize the number of tasks scheduled before a terminal state and 2) maximize the number of successful schedules. Our PT-PNT is trained on a set of 150 schedules and then with 500 episodes of DAgger. Our RI-PNT is given 650 episodes of DAgger. We find that our PT-PNT outperforms a

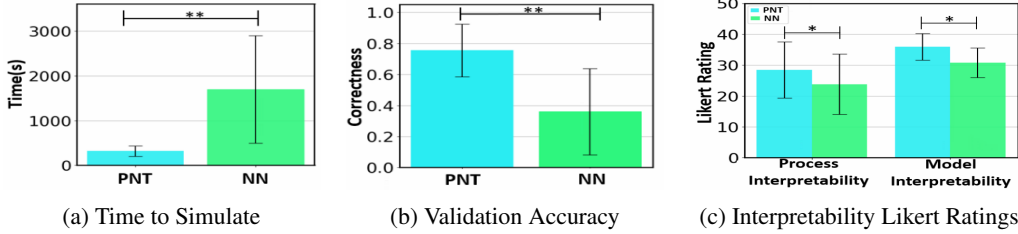


Figure 2: The findings of our user study. We find significance for hypotheses **H1**, **H2**, and **H3**.

RI-PNT by 28.57% in successful schedule completion and 12.5% in the number of tasks completed before failure. This result shows the benefits of pre-training using our framework and that our approach is amenable to DAgger-based training.

## 6 Interpretability User Study

Thus far, we have shown across a variety of datasets that our counterfactual PNT algorithm is able to achieve SOTA performance in learning from heterogeneous decision-makers. To show that our models are interpretable, we assess whether the counterfactual PNT is useful in the hands of end users. Accordingly, we conducted a novel user study to assess the interpretability of our framework. We design an online questionnaire that asks users to make predictions following each a counterfactual decision tree (PNT) and a neural network (NN). Detail about the generation of these models is in the supplementary material. We explore three hypotheses: tree-based decision-making models are more interpretable (**H1**), quicker to validate (**H2**), and are easier to simulate (**H3**) than neural networks. To test (**H1**), we ask users to answer a 13-item Likert questionnaire assessing whether the user understands the components of the decision-making model (i.e., model interpretability) and how to translate an input to an output (i.e., process interpretability) after utilizing each decision-making framework. To test (**H2**) and (**H3**), we record the time required for a user to compute the model’s output given a set of inputs, and measure the user’s ability to correctly determine the model’s output given a set of inputs, respectively.

### 6.1 User Study Results and Discussion

Our IRB-approved anonymous survey was completed by twenty adult university students. Fig. 2 depicts the results testing **H1-H3**. The complete analysis is located in the supplementary material. **H1:** We test for normality and homoscedasticity and do not reject the null hypothesis in either case, using Shapiro-Wilk ( $p > 0.3$  and  $p > 0.7$ ) and Levene’s Test ( $p > 0.5$  and  $p > 0.1$ ). We perform a paired t-test and find that tree-based models were rated statistically significantly higher than neural networks on users’ Likert scale ratings for model interpretability and overall process interpretability ( $p < 0.05$  and  $p < 0.05$ ). **H2:** We perform a Wilcoxon signed-rank test on the per-model time to determine an output and find that tree-based models were statistically significantly quicker to validate than neural networks ( $p < 0.01$ ). **H3:** We test for normality and homoscedasticity and do not reject the null hypothesis in either case, using Shapiro-Wilk ( $p > 0.2$ ) and Levene’s Test ( $p > 0.4$ ). We perform a paired t-test and find that users using tree-based models statistically significantly achieved higher overall correctness scores compared to NN based models ( $p < 0.01$ ), supporting **H3**. Given these positive results, we believe our model sets a new state-of-the-art in accuracy for heterogeneous LfD (Table 1) and also a strong step towards making such models more interpretable.

## 7 Conclusion

We present an apprenticeship scheduling framework for learning from heterogeneous demonstrators, leveraging a Personalized Neural Tree that is able to capture the homo- and heterogeneity in scheduling demonstrations through the use of personalized embeddings. The design of our PNT allows for translation into an interpretable form while maintaining a high level of accuracy. We demonstrate that our approach is notably superior to standard apprenticeship learning models and several approaches used in multi-modal behavior learning on synthetic and real-world data across three domains. Finally, we conduct a novel user study to assess the interpretability between our discretized trees and neural networks and find that our discrete trees are more interpretable ( $p < 0.05$ ), easier to simulate ( $p < 0.01$ ), and quicker to validate ( $p < 0.01$ ).

## 8 Broader Impact

Our interpretable apprenticeship scheduling framework has broad impacts on society and the learning from demonstration community. Our interpretable trees can give key insight into the behavior of a machine-learning-based agent, allowing a human to verify that safety constraints are being met and increasing the trustworthiness of the autonomous agent. Furthermore, these trees allow human operators to follow the decision step-by-step, allowing for verification [11, 18], and holding machines accountable [19].

**Beneficiaries –** Our work has the potential to benefit all human-machine collaborations, providing improved transparency, and strengthening the trustworthiness of machine teammates through policy verification. Our research contributions additionally benefit research and laboratories pursuing learning from diverse human data (which commonly contains heterogeneity).

**Negatively affected parties –** With any model, we believe it is important to gather consent before utilizing one’s data. As our model can be used by humans as both a forward model to understand decision-maker behavior and as an inverse model to infer modality, there is a possibility of discovering latent characteristics about individuals that may reflect negatively upon them.

**Implications of failure –** Failure of our approach to produce high-accuracy behavior during deployment will result in a lack of trust towards the system. In the worst case, careless application may contribute to misunderstandings causing damage from a deployed robot.

**Bias and Fairness –** The learned behavior of our PNTs will be biased towards demonstrators within the training set. If the collected set excludes certain persona, the behavior of these persona will not be represented by our PNT. However, it should be noted that as our approach is able to better take into account heterogeneity within the training data compared to other apprenticeship learning approaches. In other words, our framework is better able to represent the entire population rather than overfitting to the most prevalent demonstrator behavior than previous approaches.

**Impact on LfD community –** Personalized Neural Trees can easily be extended to a variety of domains, increasing the data-efficiency, accuracy, and utility of learning-from-demonstration with multiple human demonstrators. We demonstrate this by using a PNT to learn kinesthetic robot table tennis demonstrations. We provide details about this domain, the collection process, and the results in the supplementary material.

**Reproducibility –** Following the NeurIPS Reproducibility Checklist, we upload all code [here](#). Within this repository, we provide collected real-world datasets, code to generate synthetic data, and code to run all benchmarks. Alongside this, we attach trained models for each domain. Further in the supplementary material, we provide specifications of our hyperparameters, descriptions of our computing infrastructure, and other details regarding runtime.

## Acknowledgments and Disclosure of Funding

This work was sponsored by MIT Lincoln Laboratory grant 7000437192, the Office of Naval Research under grant N00014-19-1-2076, NASA Early Career Fellowship grant 80HQTR19NOA01-19ECF-B1, and a gift to the Georgia Tech Foundation from Konica Minolta, Inc.

## References

- [1] P. M. Berry, M. Gervasio, B. Peintner, and N. Yorke-Smith. Ptime: Personalized assistance for calendaring. *ACM Transactions on Intelligent Systems and Technology*, 2(4):40:1–40:22, July 2011.
- [2] Umang Bhatt, Alice Xiang, Shubham Sharma, Adrian Weller, Ankur Taly, Yunhan Jia, Joydeep Ghosh, Ruchir Puri, José M. F. Moura, and Peter Eckersley. Explainable machine learning in deployment, 2019.
- [3] Léon Bottou, Jonas Peters, Joaquin Quiñonero Candela, Denis X. Charles, D. Max Chickering, Elon Portugaly, Dipankar Ray, Patrice Simard, and Ed Snelson. Counterfactual reasoning and learning systems: The example of computational advertising. *J. Mach. Learn. Res.*, 14(1):3207–3260, January 2013. ISSN 1532-4435.

[4] Daniel S. Brown, Wonjoon Goo, Prabhat Nagarajan, and Scott Niekum. Extrapolating beyond suboptimal demonstrations via inverse reinforcement learning from observations. In *ICML*, 2019.

[5] David Chapman. Planning for conjunctive goals. *Artificial Intelligence*, 32(3):333 – 377, 1987. ISSN 0004-3702. doi: [https://doi.org/10.1016/0004-3702\(87\)90092-0](https://doi.org/10.1016/0004-3702(87)90092-0). URL <http://www.sciencedirect.com/science/article/pii/0004370287900920>.

[6] Letian Chen, Rohan R. Paleja, Muyleng Ghuy, and M. Gombolay. Joint goal and strategy inference across heterogeneous demonstrators via reward network distillation. *Proceedings of the 2020 ACM/IEEE International Conference on Human-Robot Interaction*, 2020.

[7] Xi Chen, Yan Duan, Rein Houthooft, John Schulman, Ilya Sutskever, and Pieter Abbeel. Infogan: Interpretable representation learning by information maximizing generative adversarial nets. In *NIPS*, 2016.

[8] Thomas G. Dietterich. Hierarchical reinforcement learning with the maxq value function decomposition. *J. Artif. Int. Res.*, 13(1):227–303, November 2000. ISSN 1076-9757.

[9] Finale Doshi-Velez and Been Kim. Towards a rigorous science of interpretable machine learning. *arXiv preprint arXiv:1702.08608*, 2017.

[10] Jakob Foerster, Gregory Farquhar, Triantafyllos Afouras, Nantas Nardelli, and Shimon Whiteson. Counterfactual multi-agent policy gradients, 2017.

[11] A. Gawande. *The Checklist Manifesto: How to Get Things Right*. Henry Holt and Company, 2010. ISBN 9781429953382. URL <https://books.google.com/books?id=x3IcNujwHxcC>.

[12] M. Gombolay, Cindy Huang, and J. Shah. Coordination of human-robot teaming with human task preferences. In *AAAI Fall Symposium Series on Artificial Intelligence for Human-Robot Interaction*, 2015.

[13] M. Gombolay, R. Jensen, Jessica Stigile, Sung-Hyun Son, and J. Shah. Apprenticeship scheduling: Learning to schedule from human experts. In *IJCAI*, 2016.

[14] Matthew Gombolay, Reed Jensen, Jessica Stigile, Sung-Hyun Son, and Julie Shah. Learning to tutor from expert demonstration via apprenticeship scheduling. In *Proceedings of the Association for the Advancement of Artificial Intelligence (AAAI) Workshop on Human-Machine Collaborative Learning (HMCL)*, San Francisco, California, February 4 2017.

[15] Matthew Gombolay, Reed Jensen, Jessica Stigile, Toni Golen, Neel Shah, Sung-Hyun Son, and Julie Shah. Human-machine collaborative optimization via apprenticeship scheduling. *Journal of Artificial Intelligence Research*, 63:1–49, 2018.

[16] Matthew C Gombolay, Reed Jensen, and Sung-Hyun Son. Machine learning techniques for analyzing training behavior in serious gaming. *IEEE Transactions on Computational Intelligence and AI in Games*, 2017.

[17] Blake Griffin. New report shows manufacturing output hit \$35 trillion in 2017, Jul 2019. URL <https://www.interactanalysis.com/new-report-shows-manufacturing-output-hit-35-trillion-in-2017-growth-forecast-to-continue/>.

[18] Alex B. Haynes, Thomas G. Weiser, William R. Berry, Stuart R. Lipsitz, Abdel-Hadi S. Breizat, E. Patchen Dellinger, Teodoro Herbosa, Sudhir Joseph, Pascience L. Kibatala, Marie Carmela M. Lapitan, Alan F. Merry, Krishna Moorthy, Richard K. Reznick, Bryce Taylor, and Atul A. Gawande. A surgical safety checklist to reduce morbidity and mortality in a global population. *New England Journal of Medicine*, 360(5):491–499, 2009. doi: 10.1056/NEJMsa0810119. URL <https://doi.org/10.1056/NEJMsa0810119>. PMID: 19144931.

[19] Alex B. Haynes, Thomas G. Weiser, William R. Berry, Stuart R. Lipsitz, Abdel-Hadi S. Breizat, E. Patchen Dellinger, Teodoro Herbosa, Sudhir Joseph, Pascience L. Kibatala, Marie Carmela M. Lapitan, Alan F. Merry, Krishna Moorthy, Richard K. Reznick, Bryce Taylor, and Atul A. Gawande. A surgical safety checklist to reduce morbidity and mortality in a global population. *New England Journal of Medicine*, 360(5):491–499, 2009. doi: 10.1056/NEJMsa0810119. URL <https://doi.org/10.1056/NEJMsa0810119>. PMID: 19144931.

[20] Fang-I Hsiao, Jui-Hsuan Kuo, and Min Sun. Learning a multi-modal policy via imitating demonstrations with mixed behaviors. *ArXiv*, abs/1903.10304, 2019.

[21] Rong Jin, Hamed Valizadegan, and Hang Li. Ranking refinement and its application to information retrieval. In *Proceedings of the 17th International Conference on World Wide Web, WWW '08*, pages 397–406, New York, NY, USA, 2008. ACM. ISBN 978-1-60558-085-2.

[22] Gary A Klein. A recognition-primed decision (rp<sub>d</sub>) model of rapid decision making. *Decision making in action: Models and methods*, 5(4):138–147, 1993.

[23] G. Ayorkor Korsah. *Exploring bounded optimal coordination for heterogeneous teams with cross-schedule dependencies*. PhD thesis, Carnegie Mellon University, Pittsburgh, PA, January 2011.

[24] Benjamin Letham, Cynthia Rudin, Tyler H McCormick, David Madigan, et al. Interpretable classifiers using rules and bayesian analysis: Building a better stroke prediction model. *The Annals of Applied Statistics*, 9(3):1350–1371, 2015.

[25] Yunzhu Li, Jiaming Song, and Stefano Ermon. Infogail: Interpretable imitation learning from visual demonstrations. In I. Guyon, U. V. Luxburg, S. Bengio, H. Wallach, R. Fergus, S. Vishwanathan, and R. Garnett, editors, *Advances in Neural Information Processing Systems 30*, pages 3812–3822. Curran Associates, Inc., 2017.

[26] Bart L MacCarthy, John R Wilson, and S Crawford. Human performance in industrial scheduling: a framework for understanding. *Human Factors and Ergonomics in Manufacturing & Service Industries*, 11(4):299–320, 2001.

[27] Microsmalldcap.com. Why tech could shakeup the \$8.1 trillion global logistics industry, Nov 2018. URL <https://www.prnewswire.com/news-releases/why-tech-could-shakeup-the-8-1-trillion-global-logistics-industry-889107785.html>.

[28] Stefanos Nikolaidis, Ramya Ramakrishnan, Keren Gu, and Julie Shah. Efficient model learning from joint-action demonstrations for human-robot collaborative tasks. In *Proceedings of the Tenth Annual ACM/IEEE International Conference on Human-Robot Interaction, HRI '15*, pages 189–196, New York, NY, USA, 2015. ACM.

[29] L. Page, S. Brin, R. Motwani, and T. Winograd. The pagerank citation ranking: Bringing order to the web. In *Proceedings of the 7th International World Wide Web Conference*, pages 161–172, Brisbane, Australia, 1998. URL [citeseer.nj.nec.com/page98pagerank.html](http://citeseer.nj.nec.com/page98pagerank.html).

[30] Tapio Pahikkala, Evgeni Tsivtsivadze, Antti Airola, Jorma Boberg, and Tapio Salakoski. Learning to rank with pairwise regularized least-squares. *SIGIR 2007 Workshop on Learning to Rank for Information Retrieval*, 01 2007.

[31] Rohan R. Paleja and Matthew Craig Gombolay. Heterogeneous learning from demonstration. *2019 14th ACM/IEEE International Conference on Human-Robot Interaction (HRI)*, pages 730–732, 2019.

[32] Geoffrey J Peter. Hands-on graduate courses in lean manufacturing (lm) emphasizing green and total productive maintenance (tpm). In *ASME 2010 International Mechanical Engineering Congress and Exposition*, pages 357–365. American Society of Mechanical Engineers Digital Collection, 2010.

[33] Herbert E. Robbins. A stochastic approximation method. *Annals of Mathematical Statistics*, 22:400–407, 2007.

[34] Stéphane Ross, Geoffrey J. Gordon, and J. Andrew Bagnell. A reduction of imitation learning and structured prediction to no-regret online learning. In *AISTATS*, 2010.

[35] Cynthia Rudin. Stop explaining black box machine learning models for high stakes decisions and use interpretable models instead, 2018.

[36] Claude Sammut, Scott Hurst, Dana Kedzier, and Donald Michie. *Learning to Fly*, page 171–189. MIT Press, Cambridge, MA, USA, 2002.

[37] Penelope M Sanderson. The human planning and scheduling role in advanced manufacturing systems: an emerging human factors domain. *Human Factors*, 31(6):635–666, 1989.

[38] Andrew Silva and Matthew Gombolay. Prolonets: Neural-encoding human experts' domain knowledge to warm start reinforcement learning. *arXiv preprint arXiv:1902.06007*, 2019.

[39] Andrew Silva, Taylor W. Killian, Ivan Dario Jimenez Rodriguez, Sung-Hyun Son, and M. Gombolay. Optimization methods for interpretable differentiable decision trees in reinforcement learning. *arXiv: Learning*, 2019.

- [40] Herbert Alexander Simon et al. *Models of a man: Essays in memory of Herbert A. Simon*. MIT Press, 2004.
- [41] Alberto Suárez and James F Lutsko. Globally optimal fuzzy decision trees for classification and regression. *IEEE Transactions on Pattern Analysis and Machine Intelligence*, 21(12):1297–1311, 1999.
- [42] Aviv Tamar, Khashayar Rohanimanesh, Yinlam Chow, Chris Vigorito, Ben Goodrich, Michael Kahane, and Derik Pridmore. Imitation learning from visual data with multiple intentions. In *International Conference on Learning Representations*, 2018.
- [43] Paul Voigt and Axel Von dem Bussche. The eu general data protection regulation (gdpr). *A Practical Guide, 1st Ed.*, Cham: Springer International Publishing, 2017.

---

# Supplementary for Interpretable and Personalized Apprenticeship Scheduling: Learning Interpretable Scheduling Policies from Heterogeneous User Demonstrations

---

Anonymous Author(s)

Affiliation  
Address  
email

## 1 Additional Experiment Domain Details

2 **Synthetic Scheduling Environment** The synthetic scheduling environment represents one of the  
 3 hardest scheduling problems. In this environment, two agents must complete a set of 20 tasks which  
 4 have upper- and lower-bound temporal constraints (i.e., deadline and wait constraints), proximity  
 5 constraints (i.e., no two agents can be in the same place at the same time), and travel-time constraints.  
 6 For the purposes of apprenticeship learning, an action is defined as the assignment of an agent to  
 7 complete a task presently. The decision-maker must decide the optimal sequence of actions according  
 8 to the decision-maker's own criteria. For this environment, we construct a set of heterogeneous, mock  
 9 decision-makers that schedule according to Equation 1.

$$\tau_i^* = \arg \max_{\tau_j \in \tau_S} (\rho_1 H_{EDF}(\tau_j) + \rho_2 H_{dist}(\tau_j) + H_{ID}(\tau_j, \rho_3)) \quad (1)$$

10 In this equation, our decision-maker selects a task  $\tau_i^*$  from the set of tasks  $\tau_S$ . The task-prioritization  
 11 scheme is based on three criteria:  $H_{EDF}$  prioritizes tasks according to deadline (i.e., “earliest-  
 12 deadline first”),  $H_{dist}$  prioritizes the closest task, and  $H_{ID}$  prioritizes tasks according to a user-  
 13 specified highest/lowest index or value based on  $\rho_3$  (i.e.,  $\rho_3(j) + (1 - \rho_3)(-j)$ ). The heterogeneity  
 14 in decision-making comes from the latent weighting vector  $\vec{\rho}$ . Specifically,  $\rho_1 \in \mathbb{R}$  and  $\rho_2 \in \mathbb{R}$   
 15 weight the importance of  $H_{EDF}$  and  $H_{dist}$ , respectively.  $\rho_3 \in \{0, 1\}$  is a mode selector in which  
 16 the highest/lowest task index is prioritized. By drawing  $\vec{\rho}$  from a multivariate random distribution,  
 17 we can create an infinite number of unique demonstrator types. This adapted environment differs  
 18 from the synthetic, low-dimensional environment in that there are a rich set of temporal, spatial, and  
 19 agent-based constraints modeling the job-shop scheduling problem; furthermore, the parameters of  
 20 the demonstrator's decision-making process is hidden and comprised of one discrete factor and two  
 21 continuous factors. In this domain, counterfactuals are generated by consider specific task information  
 22 such as availability, distance from agent, prerequisites satisfied.

23 **Real-world Data: Taxi Domain** Our environment has three locations: the village, the airport, and  
 24 the city. The taxi driver has the objective of picking up a passenger from the city or village. There is  
 25 always a passenger at the city, but the taxi driver may encounter up to 60 minutes of traffic going into  
 26 the city. There may be a wait time of up to 60 minutes to pick up a passenger at the village; however,  
 27 there is no traffic on the way to the village, and the wait time is unknown to the taxi driver unless she  
 28 is at the village. A dataset of 70 human-collected tree policies to solve this task (given with leaf node  
 29 actions such as “Drive to the City”, “Drive to the Airport”, and “Wait for Passenger”, and decision  
 30 node criterion depending on the amount of wait time, traffic time, and current location) are used to  
 31 generate heterogeneous trajectories. We originally collect 98 tree-based policies through an IRB-  
 32 approved study. However, 28 of these do not produce successful trajectories. The tree-based policies

Table 1: Apprenticeship Performance in Imitating Robot Kinesthetic Ping Pong Demonstrations.

Environment	Our Method	Sammut et al.	Nikolaidis et al.	Tamar et al.	Hsiao et. al.	InfoGAIL Li et. al.	Gombolay et. al.
Ping-Pong	<b>59.60%</b>	18.14%	31.20%	26.17%	17.96%	36.70%	28.60%

33 can be found in this GitHub repository <https://github.com/Personalized-Neural-Trees/Interpretable->  
 34 [and-Personalized-Apprenticeship-Scheduling-Learning-Interpretable-Scheduling-Policies](https://github.com/Personalized-Neural-Trees/Interpretable-).

35 **Kinesthetic Robot Table Tennis** We collected a real-world data set consisting of 10 human demon-  
 36 strators kinesthetically presenting four different table tennis strikes on a Rethink Robotics Sawyer.  
 37 The table tennis strike variants consisted of push, topspin, slice, and lob and were conducted using  
 38 a forehand motion, giving four different categories of motion. While our approach is primarily for  
 39 discrete classification problems, such as decision making, it can naturally be extended to complex  
 40 continuous domains, such as low-level robot joint control.

41 To collect data, we first show each demonstrator a sample video of the table tennis strike and allow  
 42 them to practice until she feels confident that she can return the ping pong ball over the net. Then, we  
 43 reset the robotic arm to a preset initial position and allow the demonstrator to strike a ping pong ball  
 44 launched from an automatic ball launcher. Throughout the demonstration, we record the position of  
 45 the end-effector.

46 **Survey Scheduling Environment** This domain describes a **ND[ST-SR-TA]** scheduling domain  
 47 defined by [?]. In this domain, synthetic schedulers are given utilities of three tasks where utility  
 48  $U \in \{1, 2, 3\}$  and must choose the highest or lowest task index based on a pre-specified latent  
 49 decision-making criteria. We generate a set of 100 schedules (each of length 20) from heterogeneous  
 50 demonstrators.

## 51 2 LfD Performance in Kinesthetic Robot Table Tennis

52 Here, we show that Personalized Neural Trees can easily be extended to a variety of domains,  
 53 increasing the data-efficiency, accuracy, and utility of learning-from-demonstration with multiple  
 54 human demonstrators. We demonstrate this by using a PNT to learn kinesthetic robot table tennis  
 55 demonstrations in Table 1. We received 40 demonstrations across 10 demonstrators, representing  
 56 four different table tennis strikes. To clean the trajectory of the end effector prior to learning, we  
 57 transformed our trajectories into a transformed three-dimensional space using Principal Components  
 58 Analysis. Our data was then labeled by selecting the principal component in which the end effector  
 59 moved most at each timestep ( $|\mathcal{A}| = 6$ ). As seen in row 4 of Table 1, our approach outperforms all  
 60 other benchmarks.

## 61 3 Sensitivity Analysis of PNTs

62 To analyze the sensitivity of our framework, we use our synthetic scheduling environment and perturb  
 63 the amount of data available to the PNT and the amount of noise (correctness) within the data. To  
 64 provide a thorough analysis, we validate our approach using  $k$ -fold cross-validation. This entails both  
 65 choosing a different subset of data to learn from and perturbing different truth-values of state-actions  
 66 pairs each fold.

67 As shown in Figure 1, our PNT is reasonably robust to noise for 2, 5, and 15 schedules as there is  
 68 not a steep drop in accuracy. We do not see the typical trend where the effect of noise deteriorates  
 69 as the amount of data increases. We posit the cause of this deviation as follows: As the number of  
 70 demonstrators increases, the embedding space  $\Omega$  of the PNT tends to represent a richer distribution.  
 71 While the heterogeneity among the demonstrators may remain constant (represent the same number  
 72 of modes), cases in which the PNT is unable to tease out the demonstrator mode from a single  
 73 schedule are more likely (due to the increase in the number of schedules), leading to an embedding  
 74 distribution with higher variance. Without noise, the PNT is able to make sense of the embedding  
 75 space and learn with high performance; as the amount of noise increases, it is likely more difficult to

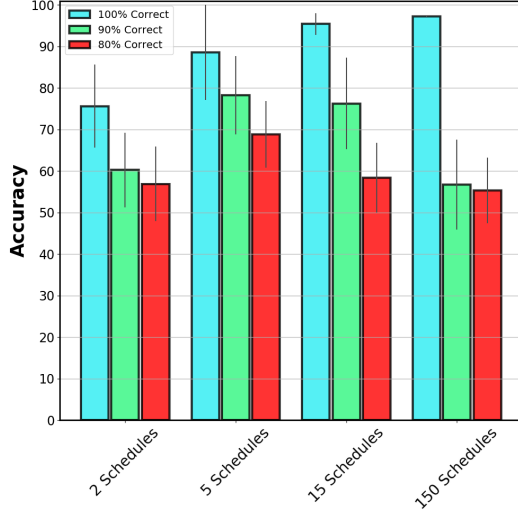


Figure 1: Sensitivity analysis in the synthetic scheduling environment.

76 represent demonstrators compactly within the embedding space. We posit that this increased variance  
 77 within the embedding space caused by the combined effect of an increased number of demonstrators  
 78 and noise leads to a reduction in performance when noise is held constant and the amount of data  
 79 increases.

80 As expected, as the number of schedules increase, the PNTs have higher accuracy. However, from  
 81 15 to 150 schedules (a 10x magnitude increase in data), for the case of 100% correct data, there is  
 82 only a  $\sim 2\%$  increase in accuracy. This result provides support to the claim of data-efficiency in our  
 83 apprenticeship scheduling framework.

#### 84 4 Evidence Lower Bound

85 Here, we present the full derivation of the evidence lower bound (ELBO) that is used to maximize the  
 86 mutual information between  $\omega$  and trajectories  $\tau$ .

$$\begin{aligned}
 G(\omega; \tau) &= H(\omega) - H(\omega|\tau) \\
 &= \mathbb{E}_{\omega \sim P(\omega), a_p^t \sim f_{\theta|\omega}^{PNT}} [\log P(\omega|s_p^t, a_p^t)] + H(\omega) \\
 &= \mathbb{E}_{a \sim f_{\theta|\omega}^{PNT}} [D_{KL}(\log(P(\omega_p|s_p^t, a_p^t)) || \log(q_{\zeta|\theta}^{\omega}(s_p^t, a_p^t))) + \mathbb{E}_{\omega \sim P(\omega)} \log(q_{\zeta|\theta}^{\omega}(s_p^t, a_p^t))] + H(\omega) \\
 &\geq \mathbb{E}_{\omega_p \sim \mathcal{N}(\mu_p, \sigma_p^2), a \sim f_{\theta|\omega}^{PNT}} [\log(q_{\zeta|\theta}^{\omega}(\omega_p|s_p^t, a_p^t))] + H(\omega) = L_G(f_{\theta|\omega}^{PNT} || q_{\zeta|\theta}^{\omega})
 \end{aligned} \tag{2}$$

87 In our approach, we make use of continuous personalized embeddings which allow for greater  
 88 expressivity in the embedding space,  $\Omega$ . As such, we utilize a mean-squared error (MSE) loss  
 89 between a sample from the approximate posterior (modeled as a normal distribution with constant  
 90 variance) and the current embedding.

91 We present the approximate normal distribution,  $\mathcal{N}_{q_{\zeta|\theta}^{\omega}}$ , in Equation 3, where  $\omega$  is the mean outputted  
 92 by the posterior network, and  $\sigma$  is the standard deviation.

$$\mathcal{N}_{q_{\zeta|\theta}^{\omega}} = \frac{1}{\sigma\sqrt{2\pi}} e^{-\frac{1}{2}\frac{(x-\omega)^2}{\sigma^2}} \tag{3}$$

93 **Theorem 4.1.** *Minimizing the mean-squared error between a sample from the approximate posterior  
 94 and the current embedding is equivalent to maximizing the log-likelihood and therefore, the evidence  
 95 lower bound.*

96 *Proof.* The mean-squared error (MSE) loss is  $(x - \omega)^2$ , where  $\omega$  is the sample from the approximate  
 97 posterior, and  $x$  is the current personalized embedding used to generate the predicted action. This is  
 98 equivalent to the exponent numerator in  $\mathcal{N}_{q_{\zeta|\theta}^{\omega}}$ . With constant variance, the exponential function is

99 monotonic, and thus, minimizing the exponent will maximize the likelihood of the posterior. Thus,  
100 minimizing the MSE is equivalent to maximizing the likelihood of the posterior. This naturally  
101 extends to the multivariate case.  $\square$

102 **4.1 Discussion on Freezing  $\theta$  During Evaluation**

103 As this learning paradigm presents a min-max objective, there may be instability in altering both  
104 parameters during evaluation. We freeze  $\theta$  to maintain a high level of mutual information among the  
105 embeddings and trajectories. Furthermore, this helps to avoid overfitting, and maintain interpretability  
106 among our discrete trees. If  $\theta$  were to be updated, the posterior network  $q_{\zeta|\theta}^{\omega}$  would need to be  
107 retrained to maintain the current level of mutual information. Similarly, the PNT was trained with  
108 regularization offline to afford a discrete tree that allows  $\omega$  to continue to vary.

109 **5 Interpretability User Study Details**

110 Here, we present the details of our novel user study to assess the interpretability of our discretized  
111 PNTs. We design an online questionnaire that asks users to predict a task to schedule given an input  
112 using a decision-tree based method and a neural-network-based method. Each user is randomly  
113 assigned a reasoning level, standard, pointwise, or counterfactual. Standard and counterfactual  
114 reasoning are discussed in the main paper. Pointwise reasoning outputs a probability of taking a  
115 certain action given a feature vector describing that action,  $x_a^t$  from state  $s^t$ , and a contextual feature  
116 vector capturing features common to all actions  $\bar{x}^t$ . We can generate pointwise features through  
117 Equation 4.

$$z^{t,p} := [\omega_p, \bar{x}^t, x_a^t], y_a^t = 1 \quad (4)$$

$$z^{t,p} := [\omega_p, \bar{x}^t, x_{a'}^t], y_{a'}^t = 0 \quad (5)$$

118 The tree and neural network-based models were trained under minimal sizes that were capable of  
119 achieving near-perfect accuracy. Tree models are learned PNTs, which are then discretized. The NN  
120 models are generated by appending personalized embeddings to a NN and following the training  
121 methodology described in Algorithm 1 from the main paper. Then, comparison weights and model  
122 weights for the discrete trees and neural networks, respectively, were rounded to the nearest 0.25.  
123 Rounding yielded  $\sim 2\%$  loss in accuracy but allowed for the survey to be conducted within a  
124 reasonable time. For each type of decision-making framework, we provide instructions for how to  
125 utilize the framework to make a prediction. The order in which the user completes the neural network  
126 portion and decision tree portion is randomized. We explore additional hypothesis: counterfactual  
127 tree-based decision-making models are more interpretable (**H4**), quicker to validate (**H5**), and are  
128 more easily utilized (**H6**) than neural-network based models of any reasoning level. We then provide  
129 further comparisons between tree-based methods of different levels of reasoning.

130 We use four metrics throughout our user study: interpretability of the decision-making model,  
131 interpretability of the overall decision-making process, time to compute an output, and correctness.  
132 To verify **H4-H6**, we must compare the counterfactual discretized PNT to a standard neural network,  
133 pointwise neural network, and pairwise neural network. As the first case is shown in the paper  
134 (standard neural network vs. discretized PNT), we provide the results for the other two scenarios  
135 here.

136 **6 Survey Results**

137 Our IRB-approved anonymous survey was sent out to adult university students. We collected 35  
138 responses, 14 of standard, 11 of pointwise, and 15 of counterfactual. We filter out responses that put  
139 in nonsensical answers (i.e., letters where numbers should be and repeated answers).

140 **H4:** In comparing a NN with pointwise reasoning to a discretized PNT, we test for normality and  
141 homoscedasticity and do not reject the null hypothesis in either case, using Shapiro-Wilk ( $p > 0.9$   
142 and  $p > 0.3$ ) and Levene's Test ( $p > 0.2$  and  $p > 0.3$ ). We perform a paired t-test and find that  
143 counterfactual tree-based models were rated statistically significantly higher than pointwise neural  
144 networks on users' Likert scale ratings for model interpretability and overall process interpretability

145 ( $p < 0.05$  and  $p < 0.01$ ). In comparing a NN with pairwise reasoning to a discretized PNT, we  
146 test for normality and homoscedasticity and do not reject the null hypothesis in either case, using  
147 Shapiro-Wilk ( $p > 0.1$  and  $p > 0.1$ ) and Levene's Test ( $p > 0.4$  and  $p > 0.4$ ). We perform a paired  
148 t-test and find that counterfactual tree-based models were rated statistically significantly higher than  
149 pointwise neural networks on users' Likert scale ratings for model interpretability and overall process  
150 interpretability ( $p < 0.01$  and  $p < .05$ ). These results support **H4**.

151 **H5:** In comparing a NN with pointwise reasoning to a discretized PNT, we perform a Wilcoxon  
152 signed-rank test on the per-model time to determine an output and find that tree-based models were  
153 not statistically significantly quicker to validate than neural networks ( $p = 0.37$ ). In comparing a  
154 NN with pairwise reasoning to a discretized PNT, we perform a Wilcoxon signed-rank test on the  
155 per-model time to determine an output and find that tree-based models were statistically significantly  
156 quicker to validate than neural networks ( $p = 0.001$ ). This result provides partial support **H5**.

157 **H6:** In comparing a NN with pointwise reasoning to a discretized PNT, we perform a Wilcoxon  
158 signed-rank test on the per-model time to determine an output and find that tree-based models were  
159 statistically significantly achieved higher overall correctness scores compared to NN based models  
160 ( $p < 0.05$ ), supporting **H6**. In comparing a NN with pairwise reasoning to a discretized PNT, we  
161 test for normality and homoscedasticity and do not reject the null hypothesis in either case, using  
162 Shapiro-Wilk ( $p > 0.05$ ) and Levene's Test ( $p > 0.2$ ). We perform a paired t-test and find that  
163 users using tree-based models statistically significantly achieved higher overall correctness scores  
164 compared to NN based models ( $p < 0.001$ ), supporting **H6**.

## 165 7 Hyperparameters and Architecture Details

166 We compare our personalized apprenticeship scheduling approach to several baselines [? ? ? ? ? ].  
167 Throughout this section, we will discuss the architecture, implementation details, and learning rates  
168 for all baselines and our algorithm in each domain. The runtime mentioned is in respect to a desktop  
169 with a NVIDIA RTX 2080Ti GPU and an Intel i7 processor.

### 170 7.1 Synthetic Low-Dimensional Environment

171 Each apprenticeship learning algorithm below is given 50 schedules to learn from and tests on a set  
172 of 50 unseen demonstrations.

- 173 • For the method of [? ], we utilize an multi-layer perceptron (MLP) with 3 linear layers  
174 connected by ReLU activation functions. After the last linear layer, we utilize a log softmax  
175 function to compute the log probability of which task to schedule. Each linear layer has 10  
176 hidden units. We utilize the Adam optimizer with a learning rate of  $1e^{-3}$ . The runtime for  
177 training and verifying this model is under 30 minutes.
- 178 • For the method of [? ], we utilize k-means clustering to separate the data into two clusters.  
179 Two neural networks (one for each cluster) are trained to imitate demonstrator data within  
180 the cluster. Each network utilizes the same architecture and learning rate used in the baseline  
181 of [? ]. The runtime for training and verifying this model is under 30 minutes.
- 182 • For the method of [? ], we utilize an simulator-free version of infoGAIL. The policy,  
183 discriminator, and approximate posterior are modeled by MLPs with 2 linear layers (32  
184 hidden units) connected by a ReLU activation function, and an output activation function of  
185 a softmax, sigmoid, and softmax respectively. We initialize the number of discrete modes  
186 to 2. We utilize learning rates of  $1e^{-4}$ ,  $1e^{-3}$ ,  $1e^{-4}$  respectively. For the hyperparameters  
187 of infoGAIL, we initialize  $\lambda_1$  to 1,  $\gamma$  to 0.95, and  $\lambda_2$  to 0. The runtime for training and  
188 verifying this model is under 30 minutes.
- 189 • For the method of [? ], we utilize a neural network with 3 linear layers (10, 2, 2 hidden  
190 units, respectively) connected by ReLU activation functions. We use N=5 samples as our  
191 hyperparameter to estimate the intention probability distribution  $\mathcal{P}(z)$ . We utilize a learning  
192 rate of  $1e^{-3}$  alongside Stochastic Gradient Descent (SGD). The runtime for training and  
193 verifying this model is under 30 minutes.
- 194 • For the method of [? ], we utilize a bidirectional LSTM with attention followed by a linear  
195 layer as specified in their paper. For the decoder, we utilize three linear layers connected by

196 ReLU activation functions. We utilize a learning rate of  $1e^{-3}$  alongside Stochastic Gradient  
197 Descent (SGD). The runtime for training and verifying this model is under 30 minutes.

198 • For the method of [?], we utilize a standard decision tree (counterfactuals are not possible  
199 when  $|A| \leq 2$ ) of depth 10. The runtime for training and verifying this model is under 30  
200 minutes.

201 • For our Personalized Neural Trees, we utilize a max depth of 6 (32 leaves) and embedding  
202 dimension of 2 ( $d = 2$ ). We set learning rates of  $\theta$  to  $1e^{-3}$ ,  $\omega$  to  $1e^{-2}$ , and  $\zeta$  to  $1e^{-3}$ .  
203 We find empirically that setting the learning rate of  $\omega$  slightly higher allows for better LfD  
204 accuracy. For our approximate posterior,  $q_{\zeta|\theta}^{\omega}$ , we set the value of  $\sigma_p$  to zero. The runtime  
205 for training and verifying this model is under 30 minutes.

206 **7.2 Synthetic Scheduling Environment**

207 Each apprenticeship learning algorithm below is given 150 schedules to learn from and tests on a set  
208 of 100 unseen demonstrators.

209 • For the method of [?], we utilize an multi-layer perceptron (MLP) with six linear layers  
210 connected by ReLU activation functions. After the last linear layer, we utilize a log softmax  
211 function to compute the log probability of which task to schedule. Each linear layers have  
212 128, 128, 32, 32, 32, and 20 hidden units, respectively. We utilize the Adam optimizer with  
213 a learning rate of  $1e^{-4}$ . The runtime for training and verifying this model is approximately  
214 30 minutes.

215 • For the method of [?], we utilize k-means clustering to separate the data into three clusters.  
216 Three neural networks (one for each cluster) are trained to imitate demonstrator data within  
217 the cluster. Each network utilizes the same architecture and learning rate used in the baseline  
218 of [?]. The runtime for training and verifying this model is approximately 30 minutes.

219 • For the method of [?], we again utilize a simulator-free version of infoGAIL. The policy  
220 follows the same network structure used in the [?] baseline. The discriminator and approxi-  
221 mate posterior are modeled by MLPs with six linear layers (128, 128, 128, 32, 32, 32 hidden  
222 units, respecitively) connected by a ReLU activation function, and an output activation  
223 function of a sigmoid, and softmax respectively. We initialize the number of discrete modes  
224 to 3. We utilize learning rates of  $1e^{-4}$ ,  $1e^{-3}$ ,  $1e^{-4}$  respectively. For the hyperparameters  
225 of infoGAIL, we initialize  $\lambda_1$  to 1,  $\gamma$  to 0.95, and  $\lambda_2$  to 0. The runtime for training and  
226 verifying this model is approximately 24-48 hours.

227 • For the method of [?], we utilize a neural network with 5 linear layers (128, 32, 32, 32, 32,  
228 20, 2, 2 hidden units, respectively) connected by ReLU activation functions. We use N=5  
229 samples as our hyperparameter to estimate the intention probability distribution  $\mathcal{P}(z)$ . We  
230 utilize a learning rate of  $1e^{-3}$  alongside Stochastic Gradient Descent (SGD). The runtime  
231 for training and verifying this model is approximately 3 hours.

232 • For the method of [?], we utilize a bidirectional LSTM with attention followed by a linear  
233 layer as specified in their paper. For the decoder, we utilize six linear layers connected by  
234 ReLU activation functions. We utilize a learning rate of  $1e^{-3}$  alongside Stochastic Gradient  
235 Descent (SGD). The runtime for training and verifying this model is approximately 3 hours.

236 • For the method of [?], we utilize a pairwise decision tree of depth 10. The counterfactuals  
237 are set to one-hot encodings of each action, as done in the original paper. The runtime for  
238 generating and verifying this model is approximately 5 minutes.

239 • For our Personalized Neural Trees, we utilize a max depth of six (32 leaves) and embedding  
240 dimension of 3 ( $d = 3$ ). We set learning rates of  $\theta$  to  $1e^{-2}$ ,  $\omega$  to  $1e^{-2}$ , and  $\zeta$  to  $1e^{-2}$ . We  
241 find empirically that pretraining the policy network first and then adding in the posterior  
242 at a later epoch results in both good performance and mutual information maximization.  
243 This is opposed to training both models at once from scratch. For our approximate posterior,  
244  $q_{\zeta|\theta}^{\omega}$ , we set the value of  $\sigma_p$  to zero. The runtime for training and verifying this model is  
245 approximately 24 hours.

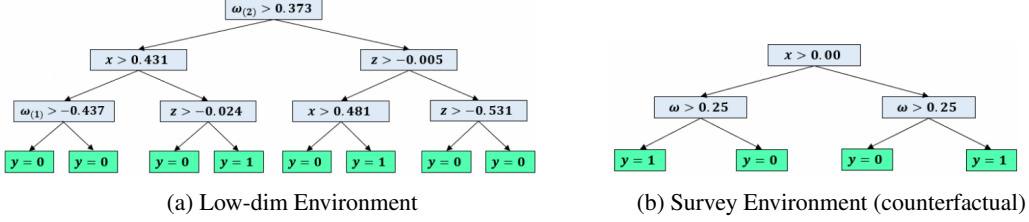


Figure 2: This figure depicts the learned PNT model after translation to an interpretable form.

246 **7.3 Taxi Domain**

247 Each apprenticeship learning algorithm below is given 25 successful trajectories from each user and  
 248 tested on a set of 25 unseen trajectories from each demonstrator.

- 249 • For the method of [? ], we utilize the same architecture and learning rate as that of the  
 250 synthetic scheduling environment. The runtime for training and verifying this model is  
 251 approximately 30 minutes.
- 252 • For the method of [? ], we utilize k-means clustering to separate the data into three clusters.  
 253 Three neural networks (one for each cluster) are trained to imitate demonstrator data within  
 254 the cluster. Each network utilizes the same architecture and learning rate used in the baseline of [? ]. The runtime for training and verifying this model is approximately 30 minutes.
- 255 • For the method of [? ], we utilize the same architecture and learning rate as that of the  
 256 synthetic scheduling environment. The runtime for training and verifying this model is  
 257 approximately 24-48 hours.
- 258 • For the method of [? ], we utilize the same architecture and learning rate as that of the  
 259 synthetic scheduling environment. The runtime for training and verifying this model is  
 260 approximately 3 hours.
- 261 • For the method of [? ], we utilize the same architecture and learning rate as that of the  
 262 synthetic scheduling environment. The runtime for training and verifying this model is  
 263 approximately 3 hours.
- 264 • For the method of [? ], we utilize a pairwise decision tree of depth 13. The counterfactuals  
 265 are set to one-hot encodings of each action, as done in the original paper. The runtime for  
 266 generating and verifying this model is approximately 5 minutes.
- 267 • For our Personalized Neural Trees, we utilize a max depth of 8 (128 leaves) and embedding  
 268 dimension of 3 ( $d = 3$ ). As counterfactual task information is not readily available, we  
 269 utilize one-hot encodings for each action. We set learning rates of  $\theta$  to  $1e^{-2}$ ,  $\omega$  to  $1e^{-1}$ ,  
 270 and  $\zeta$  to  $1e^{-2}$ . We find empirically that pretraining the policy network first and then adding  
 271 in the posterior at a later epoch results in both good performance and mutual information  
 272 maximization. For our approximate posterior,  $q_{\zeta|\theta}^{\omega}$ , we set the value of  $\sigma_p$  to zero. The  
 273 runtime for training and verifying this model is approximately 12 hours.

275 **8 Interpretable Models**

276 As machine learning is being increasingly deployed into the real world, interpretability is required  
 277 for these systems to gain human trust [? ? ? ]. Interpretability refers to attempts that help the user  
 278 understand why a machine learning model behaves the way it does. A clear visualization of a policy  
 279 is one way to help a human form an accurate representation of its capabilities [? ]. Furthermore,  
 280 an interpretable model of resource allocation or planning tasks would be highly useful for a variety  
 281 of reasons, from decision explanations to training purposes. In Figure 2, we display interpretable  
 282 models generated through discretization for the low-dimensional environment and survey scheduling  
 283 environment.

284 **9 Future Work**

285 During the deployment of a discretized PNT, we required pre-inferred embeddings to understand  
286 decision-maker behavior. As this involves a sample of the decision-maker’s data and the use of  
287 backpropagation with a pre-discretized PNT to infer demonstrator style, we feel this can be improved  
288 by producing the demonstrator embedding through the means of our approximate posterior  $q_{\zeta|\theta}^{\omega}$ ,  
289 modeled as a  $PNT \setminus \omega$ . This can be discretized following the framework of Section 4.3 of our paper,  
290 producing an interpretable model that predicts a mean and covariance of an embedding given a single  
291 state-action pair. This discretized posterior then takes in a state-action pair and produce the latent  
292 embedding that generated this action. In this way, the interpretable discretized PNT has a method to  
293 naturally infer the demonstrator’s embedding.